Journal of Photochemistry & Photobiology, A: Chemistry 456 (2024) 115866

Contents lists available at ScienceDirect

Journal of Photochemistry & Photobiology, A: Chemistry

journal homepage: www.elsevier.com/locate/jphotochem

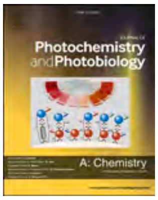

Efficiency enhancement of photovoltaic cells under infrared light irradiation by synergistic upconversion luminescence of $NaYF_4:Yb^{3+}/Er^{3+}/Tm^{3+}@TiO_2$-CQDs

Shaoqi Zhu [a,b], Xiaofeng Xie [a,b,*], Xiaoyu Duan [a], Guanqing Song [a,b], Guanhong Lu [a], Yan Wang [a], Jing Sun [a,b,*]

[a] Shanghai Institute of Ceramics, Chinese Academy of Sciences, 585 Heshuo Road, Shanghai, China
[b] University of Chinese Academy of Sciences, 19 Yuquan Road, Beijing, China

ARTICLE INFO

Keywords:
Photovoltaic cell
Infrared light
Upconversion
Rare-earth
CQDs

ABSTRACT

Rare-earth doped upconversion luminescence (UCL) is of great significance in improving the utilization of infrared (IR) light from solar radiation, especially in the efficiency enhancement of photovoltaic (PV) cells. However, the low level of luminescence efficiency remains a great challenge. Here, we designed $NaYF_4:Yb^{3+}/Er^{3+}/Tm^{3+}@TiO_2$-CQDs upconversion luminescent materials. The construction of the core–shell structure and the loading of carbon quantum dots (CQDs) resulted in a 9-fold enhancement of upconversion luminescence and a 3.02% enhancement of the efficiency of the photovoltaic cell. These data indicate that the construction of the core–shell structure can effectively inhibit the surface quenching of the luminescent particles, and that the energy transfer between the carbon quantum dots and the rare earth ions has a synergistic effect on the efficiency enhancement of the photovoltaic cell. Meanwhile, the TiO_2 shell layer also enables the prepared materials to have better properties of self-cleaning and degradation of organic pollutants, which will further improve the visible light utilization of PV cells. $NaYF_4:Yb^{3+}/Er^{3+}/Tm^{3+}@TiO_2$-CQDs provides new ideas for the practical application of PV cell efficiency enhancement and the design of new materials.

1. Introduction

New energy is one of the key directions of research and development in the word, and PV power generation has become the main force for the optimization of the energy pattern [1]. Improving the efficiency of PV is one of the focuses of current research [2]. However, during the prolonged use of PV modules, the accumulation of dust and pollutants can hinder the absorption of incident light by PV cells, which in turn greatly reduces the efficiency of PV power generation [3]. At the same time, Due to the limitations of the photovoltaic cell bandgap, its spectral response is in the wavelength range of 320–1100 nm, while the infrared light, which accounts for about 43 % of solar radiation, is underutilized [4]. To further improve the efficiency of PV, it is essential to develop an innovative material to solve the problems of dust accumulation and IR photons utilization.

Compared with the high cost of manual regular cleaning of the surface of PV modules, self-cleaning materials are a more favorable choice for surface dirt removal, which have been widely studied (such as TiO_2) and commercialized in recent years [5]. But combining self-cleaning materials with UCL materials that could convert IR with low-energy photons to visible with high-energy photons has been little studied, which will have good application potential in PV efficiency enhancement [6]. UCL materials with rare-earth doping have received widespread consideration for their superior properties, such as excellent photostability, rich ladder energy levels, sharp emission lines, and large anti-Stokes shifts [7,8]. UCL materials are widely used in many application areas [9], including bioimaging [10], optical sensing [11], anti-counterfeiting [7], and catalysts [12], and so on. However, low luminescent intensity and easy quenching often limit their practical application [13]. Thus, many strategies have been developed to improve the intensity and efficiency of UCL, such as impurity ion doping [14], plasma resonance [15], core–shell structure construction [16], photon crystal [17], and dye sensitization [18,19]. Among these strategies, the coating of inert shell in core–shell structure can reduce fluorescence quenching and enhance UCL by effectively passivating surface defects [20]. Huang et al. designed $NaYF_4:Gd@NaYbF_4:Tm@NaYF_4$

---

* Corresponding authors.
E-mail addresses: xxfshcn@163.com (X. Xie), jingsun@mail.sic.ac.cn (J. Sun).

https://doi.org/10.1016/j.jphotochem.2024.115866
Received 26 May 2024; Received in revised form 14 June 2024; Accepted 26 June 2024

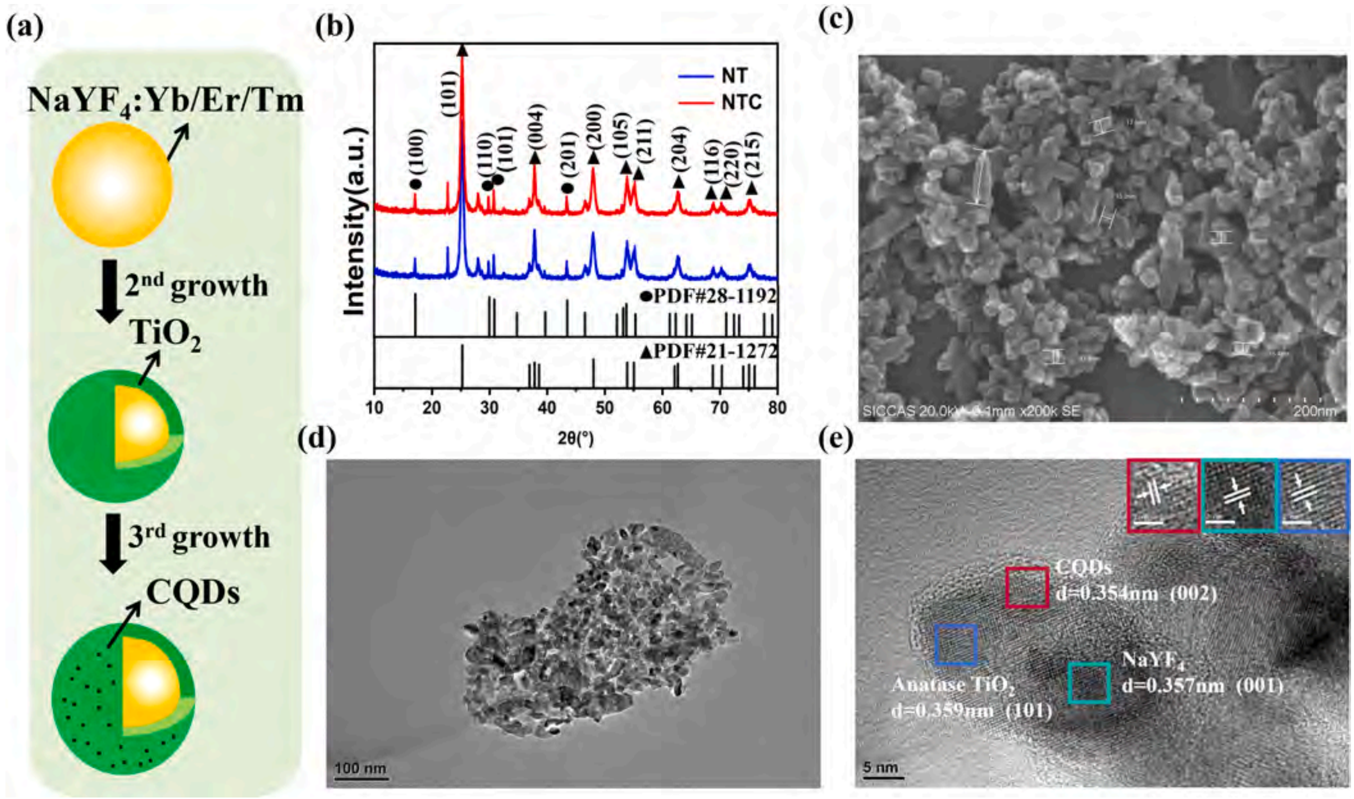

Fig. 1. (a) Preparation process of NTC. (b) XRD, (c) SEM, (d) TEM, (e) HRTEM.

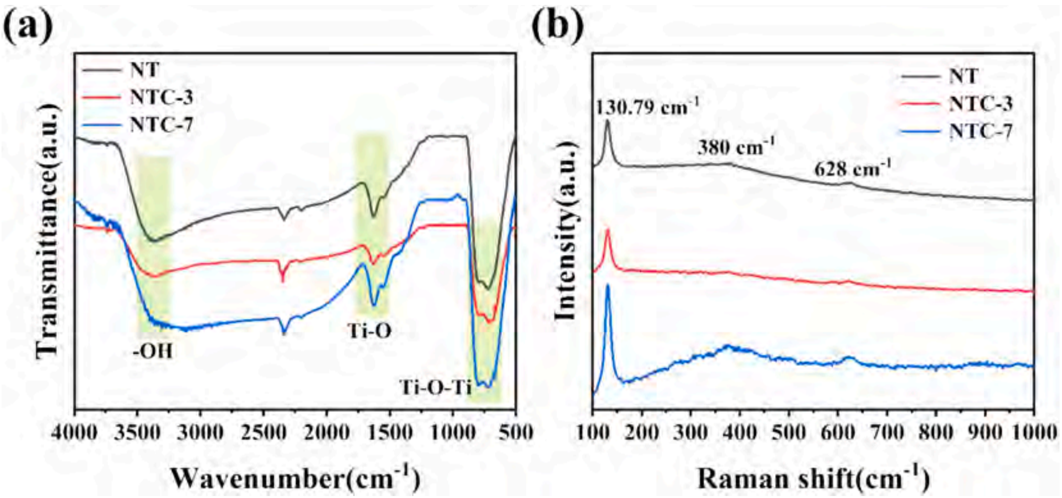

Fig. 2. (a) FT-IR spectra and (b) Raman spectra of NT, NTC-3, and NTC-7.

multilayered structure to realize upconversion with switching colors and wide emission range [21]. Tian et al. grew a fluorinated oxygen layer YOF: Yb^{3+}/Er^{3+} in situ on $NaYF_4$:Yb^{3+}/Er^{3+} by high-temperature air annealing. The shell layer suppressed surface bursting and moderated the phonon energy of the host, resulting in an increase of more than 25-fold in the intensity of the upconversion emission [22]. Therefore, using self-cleaning materials as inert shell of UCL materials will achieve performance coupling in terms of PV efficiency enhancement.

However, to achieve excellent luminescence properties, the construction of the core–shell structure usually requires complex preparation [9]. It is feasible to optimize the properties of core–shell UCL materials by a simple method. Carbon quantum dots (CQDs) are widely used in photovoltaic devices, sensors and photocatalysis due to their photoinduced electron transport and luminescence properties [23–25]. By controlling their size and surface functional groups, CQDs could emit different wavelengths to fulfill various applications [26]. Liu et al. synthesized red-emissive C-dots with broad absorption (300 ~ 600 nm) and red emission (595 nm), which enabled luminescent solar concentrators exhibited optimized external optical efficiency (4.81 %) and power conversion efficiency (2.41 %) [27]. Xu et al. reported an overlap between the upconversion emission spectra of $NaYF_4$: Yb, Tm and the UV–visible absorption spectra of carbon dots (CDs) at ~ 360 nm, suggesting that energy transfer may have occurred [28]. Coupling of CQDs with high fluorescence properties at the surface of core–shell structure may be an achievable way to realize effective light absorption and excellent luminescence performance for PV efficiency enhancement.

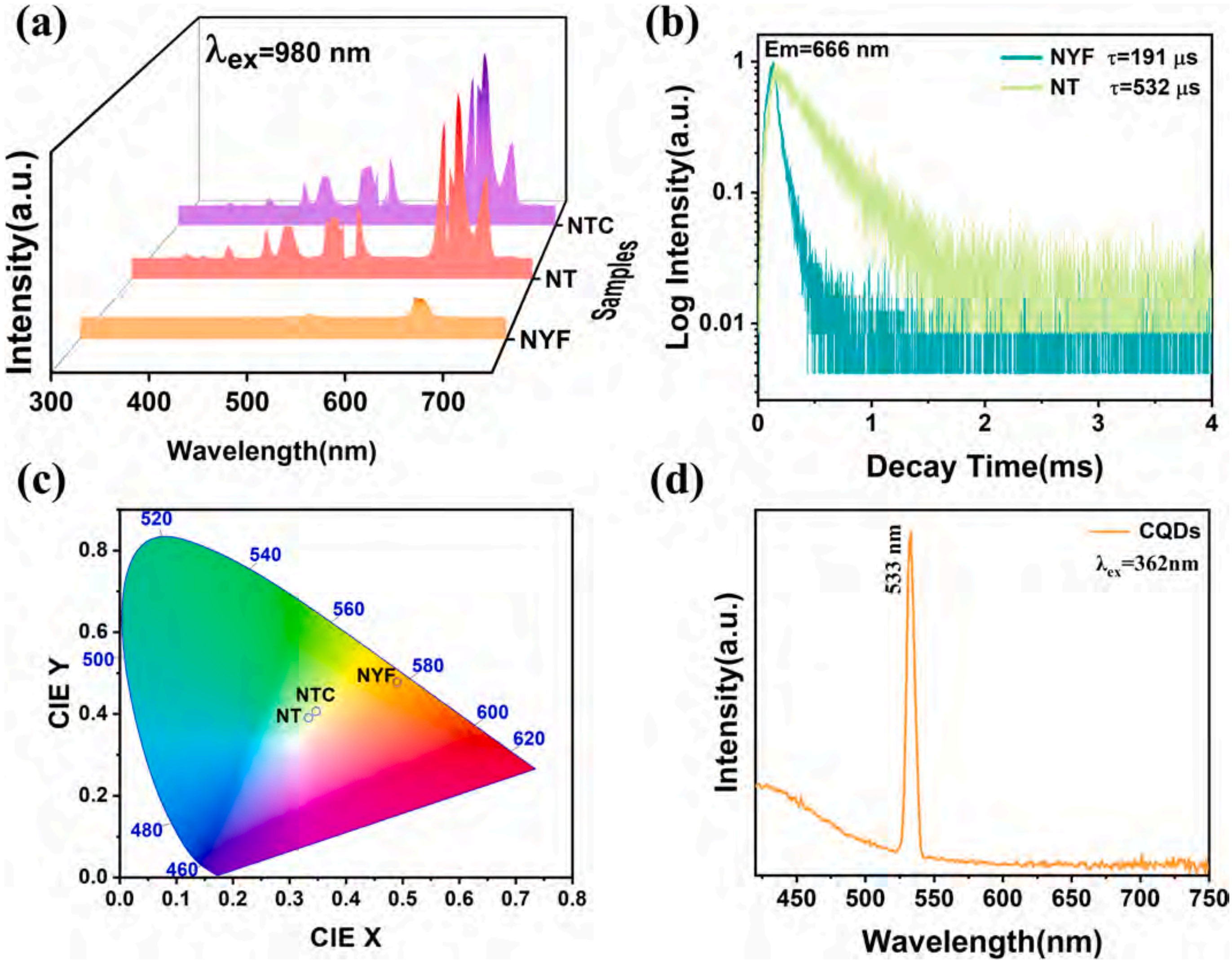

Fig. 3. (a) Upconversion luminescence spectra of the NYF, NT and NTC samples under 980 nm laser excitation. (b) Upconversion emission fluorescence lifetime spectra. (c) CIE coordinates of the emission colors of (a) samples under 980 nm excitation. (d) Down-conversion luminescence spectra of CQDs under 362 nm excitation.

Herein, we prepared $NaYF_4$:Yb^{3+}/Er^{3+}/Tm^{3+}@TiO_2-CQDs (labeled as NTC) by hydrothermal and calcination methods. Specifically, CQDs are introduced to the surface of a TiO_2-coated $NaYF_4$ (Yb^{3+} as sensitizer, Er^{3+} and Tm^{3+} as activator). Characterization and testing have confirmed that NTC not only has excellent upconversion luminescence performance, but also has good electron-hole separation ability. We further optimized the properties of this composite and explored the synergistic luminescence mechanism between rare-earth ions and CQDs. Finally, we used the prepared luminescent material to form a coating on the surface of photovoltaic modules to explore the effect on photovoltaic efficiency and tested its self-cleaning and photocatalytic properties.

2. Experimental

2.1. Materials

Diethylenetriamine ($C_4H_{13}N_3$), $Ln(NO_3)_3·6H_2O$ (Ln = Yb, Er, Tm), Yttrium (III) Nitrate Hexahydrate ($Y(NO_3)_3·6H_2O$), Sodium Fluoride (NaF), Urea (NH_2CONH_2), Citric acid monohydrate ($C_6H_8O_7·H_2O$), Titanium tetraisopropoxide ($C_{12}H_{28}O_4Ti$), and 2-Propanal ($(CH_3)_2CHOH$) were purchased from Shanghai Titan Scientific Co., Ltd. Ethanol absolute was obtained from Shanghai Lingfeng Chemical Reagent Co., Ltd. All chemicals are not further purified during use.

2.2. Preparation of NTC nanoparticles

$NaYF_4$:Yb^{3+}/Er^{3+}/Tm^{3+} (labeled as NYF) was synthesized based on a hydrothermal method [29]. The preparation of shell (NYF@TiO_2): as-obtained 0.05 g of NYF as precursor and 0.04 mL Diethylenetriamine were dispersed in the 42 mL of 2-Propanal and fully stirred for 10 min. Then, 2 mL Titanium tetraisopropoxide was added under continuous agitation and agitated continuously for an hour. The hydrothermal reaction condition was 200 °C and the reaction time was 24 h. Finally, the final product NYF@TiO_2 (named as NT) was obtained by washing, drying and further calcination (temperature and time: 350 °C, 2 h).

The introduction of CQDs: CQDs was synthesized based on a hydrothermal method [30]. The prepared NYF@TiO_2 was dissolved in ethanol (solution A), CQDs was dispersed in deionized water (solution B). Added solution B to A slowly drip and magnetically agitated to dry. The calcination condition was 300 °C, 3 h. The final product was obtained by washing and drying to get NTC-x (x = 1, 3, 5, 7). The TiO_2-CQDs (labeled as TC-x (x = 1, 3, 5, 7)) microspheres without NYF were also synthesized in a similar way. The x indicated the amount fraction of CQDs.

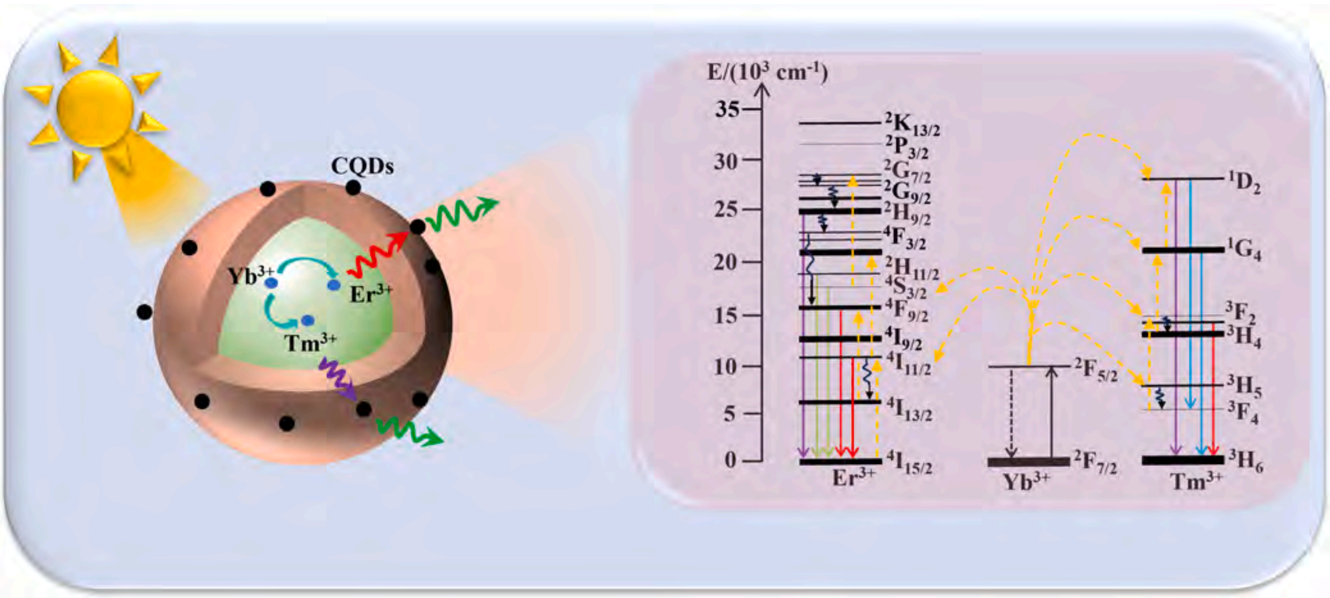

Fig. 4. The function mechanism of the synergistic UCL process in $NaYF_4$:Yb^{3+}/Er^{3+}/Tm^{3+}@TiO_2-CQDs.

2.3. *Characterization*

The crystal structures of the samples were investigated by X-ray diffractometer (XRD, D8 ADVANCE, Bruker, Germany). The surface morphology of the samples was characterized by a high emission field resolution scanning electron microscope (SEM, Verios G4, FEI Corporation, America). The morphology and core–shell structure were observed on a field emission transmission electron microscope (TEM, JEM-2100F, JEOL, Japan). The element distribution of the core–shell structure was observed on a condenser aberration-corrected transmission electron microscope (EDS, Hitachi-HF5000, Japan). The surface valence state analysis of the samples was investigated by X-ray photoelectron spectrometer (XPS, ESCAlab250, Thermo Fisher Scientific, Britain). The optical absorption properties of the samples were measured by a UV–Vis-NIR spectrophotometer (Perkin Elmer, model LAMBDA 1050). The upconversion luminescence were measured under 980 nm excitation using a low temperature absorption spectrometer (FLS-1000, Edinburgh, Britain). The photoluminescence (PL) was measured by the luminescence spectrometer (model LS 55, Perkin Elmer). The structure information of the samples was measured by an Infrared spectrometer (Spotlight400, PE Corporation, America) and a Raman microscope (DXR, Thermo Fisher Scientific, America). The transient photocurrent of the samples was tested by a photoelectrochemical workplace (CHI650b, Shanghai Chen Hua Instruments). The light transmittance of the samples was measured by a transmissivity test apparatus (SDR851).

2.4. *Preparation of coatings and IV characteristics of PV tests*

The sample was added into ethanol to form a uniformly dispersed solution with a mass ratio of 1:100. The non-woven fabric was immersed in the solution and then the solution was evenly coated on a clean glass sheet by gently pressing the non-woven fabric with the hand. The glass sheet is dried to obtain a coating with the sample. The silicon cell was commercially available crystalline silicon solar cell (polycrystalline silicon drop sheet, 4 × 4 cm). The PV cover glass coated with the sample was placed on the silicon cell to form a mini-modules.

The I-V characteristics of PV mini-modules coated with the samples were measured by a solar simulator (ProMoSim evo3, Strama-MPS, Germany) with 1 sun illumination (AM1.5G, 100 mW/cm^2). To study the effect of the prepared upconversion luminescent coating on the utilization of IR light by photovoltaic cells, we tested the coating by placing a filter on it to filter out UV and visible light at wavelengths less than 760 nm (details of the installation are shown in Fig. S1).

2.5. *Self-cleaning and photocatalytic tests*

The static contact angle of the coatings was tested using a contact angle meter (JY-82A, Chengde Dingsheng Co., Ltd). Volatile organic pollutants (VOCs), such as acetaldehyde, are key air pollutants for control. We explored the photocatalytic degradation performance of the prepared materials using acetaldehyde as the target. The adsorption and photodegradation properties of acetaldehyde were analyzed by a gas reaction device for flow phase. The process is as follows: the prepared 0.05 g sample was dissolved in ethanol and grinded thoroughly with an alumina mortar. Then, the solution was absorbed by an eyedropper to evenly apply to the clean glass (7 × 14 cm). The glass coated with sample was placed in the gas reaction chamber for testing. The photocatalytic degradation of acetaldehyde was performed when adsorption was in equilibrium. The concentration of acetaldehyde was 25 ppm and the flow rate was 20 sccm. We use a 500 W xenon lamp as the light source.

3. Results and discussion

The synthesis of NTC consists of three main steps (Fig. 1a). NYF microspheres were synthesized based on the previous report [29,31]. The core–shell structure was constructed by coating a titanium dioxide shell on the surface of UCL nanoparticles by hydrothermal and calcination method. Subsequently, the CQDs were distributed in a dispersed state on the surface of core–shell structure.

As shown in XRD pattern (Fig. 1b), the obtained NT and NTC-3 both preserved the original crystal of $Na(Y_{0.5}Yb_{0.39}Er_{0.04})F_4$ and anatase TiO_2 corresponding to PDF#28–1192 and PDF#21–1272. Besides, the introduction of CQDs did not result in impurity peaks, and the compounds maintained a high phase purity. This indicates the successful preparation of the composite materials. The SEM morphology image of NTC-3 is shown in Fig. 1c. The nanoparticles are spherical with the size of 15 nm and some grow into rods with the length of 70 nm. The morphology image and core–shell structure are measured by TEM and HRTEM of NTC-3 (Fig. 1d, e). The HRTEM image suggests the interlayer spaces of 0.359 nm, which matches to the main (1 0 1) plane of anatase TiO_2 [30].

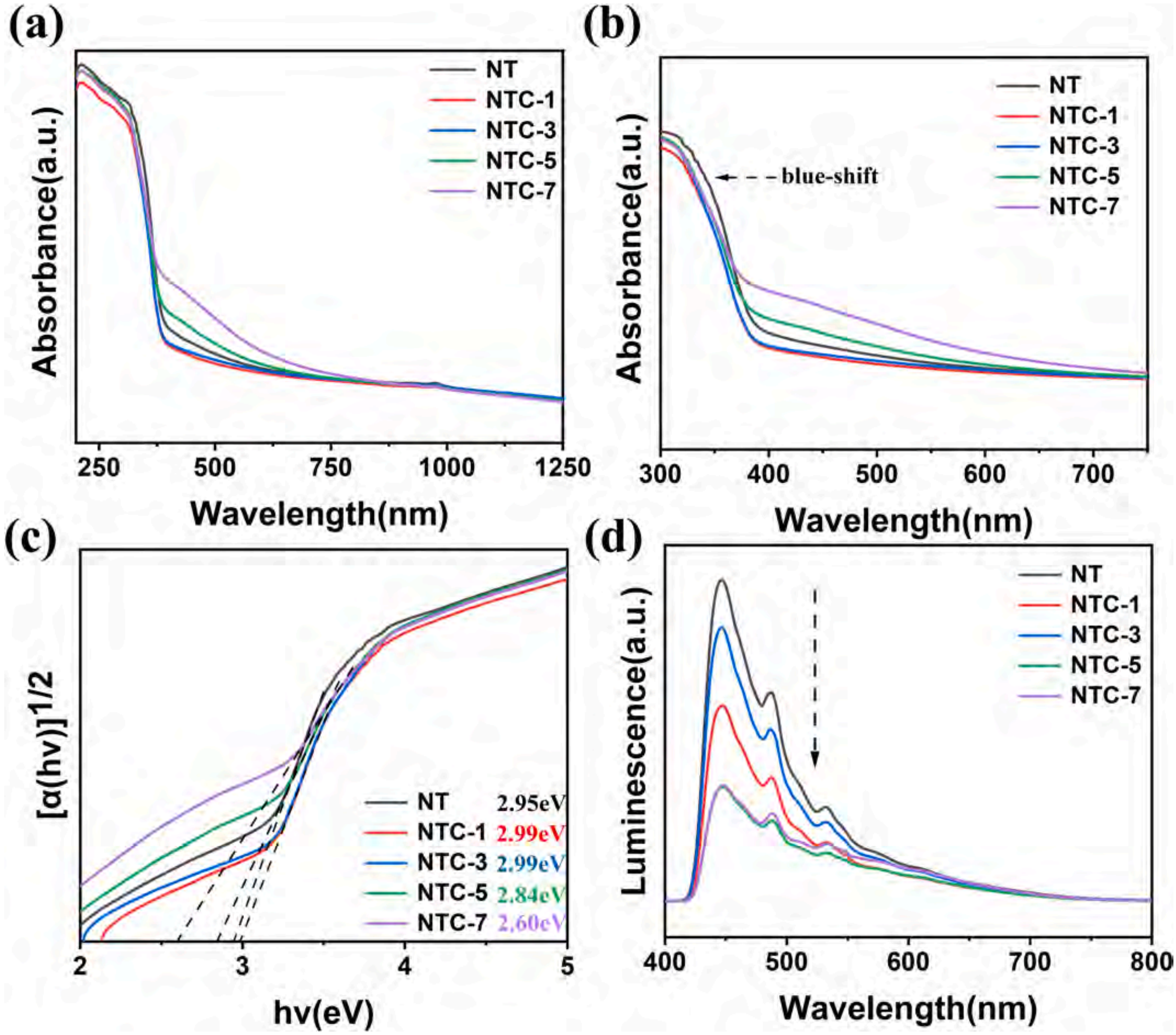

Fig. 5. (a) and (b) UV–Vis-IR diffuse reflectance spectra of NT and NTC-x samples, (c) Tauc plots of NT and NTC-x samples, (d) Photoluminescence spectra of NT and NTC-x samples under 360 nm excitation.

Besides, the interlayer spaces of 0.357 nm and 0.354 nm match to the (0 0 1) plane of $NaYF_4$ and the (0 0 2) plane of CQDs, respectively. The element mappings in Fig. S2 display the existences of C, O, Ti, Y, Na, F, Er, Yb, and Tm, which indicated a uniform distribution of elements in the UCL nanoparticles [32].

The XPS spectra of NTC-3 is shown in Fig.S3. The survey spectrum reveals the elemental composition of the NTC-3 sample in terms of F 1 s, O 1 s, Ti 2p, N 1 s, C 1 s, Yb 4b and Y 3d (Fig. S3a). The most abundant elements are Ti and O, indicating that TiO_2 is the main constituent of the prepared sample. However, the elements Er and Tm were not detected because they were below the detection limit. The peaks of Ti 2p1/2 and Ti 2p3/2 of NTC-3 were located at 464.55 eV and 458.75 eV in Fig. S3b, respectively, which were assigned to typical TiO_2 [33]. While the peaks located at 529.95 eV and 285 eV can be assigned to O 1 s and C 1 s, respectively (Fig. S3c, d).

To investigate the chemical bonding of the synthesized UCL nanoparticles and the chemical environment in which they are embedded, we performed FT-IR and Raman characterization. As shown in Fig. 2a, the peaks located at 3372 cm^{-1}, 1616 cm^{-1}, and 717 cm^{-1} are ascribed to –OH, Ti-O and Ti-O-Ti bonds, respectively [34]. And the peak located at 2333 cm^{-1} can be attributed to the stretching vibrational absorption peak of the accumulated double bond (C = O = C), which indicating that the TiO_2 and CQDs in the samples were connected through C = O and C-O bonds. Compared with the peak intensities of NT and NTC-7, the signal intensity of the NTC-3 sample is significantly weaker, which indicates that the number of surface functional groups tends to increase and then decrease with the loading of CQDs. Raman spectra of as-prepared NT, NTC-3, and NTC-7 is shown in Fig. 2b. There are three distinct characteristic peaks at 130.79 cm^{-1}, 380 cm^{-1}, and 628 cm^{-1}, which attributed to the E_g, B_{1g}, and B_{2g} vibrational modes of TiO_2, respectively [33].

Fig. 3a shows the upconversion luminescence spectra under a 980 nm laser excitation. From the figure, NYF absorbs photons at 980 nm and emits visible light at 660 nm through upconversion luminescence, which has a low intensity and a single wavelength. After coating the TiO_2 layer, the luminescence intensity is obviously enhanced (the luminescence at 660 nm is enhanced by 9 times), and the wavelength range of the photons emitted covers the ultraviolet to visible region. The

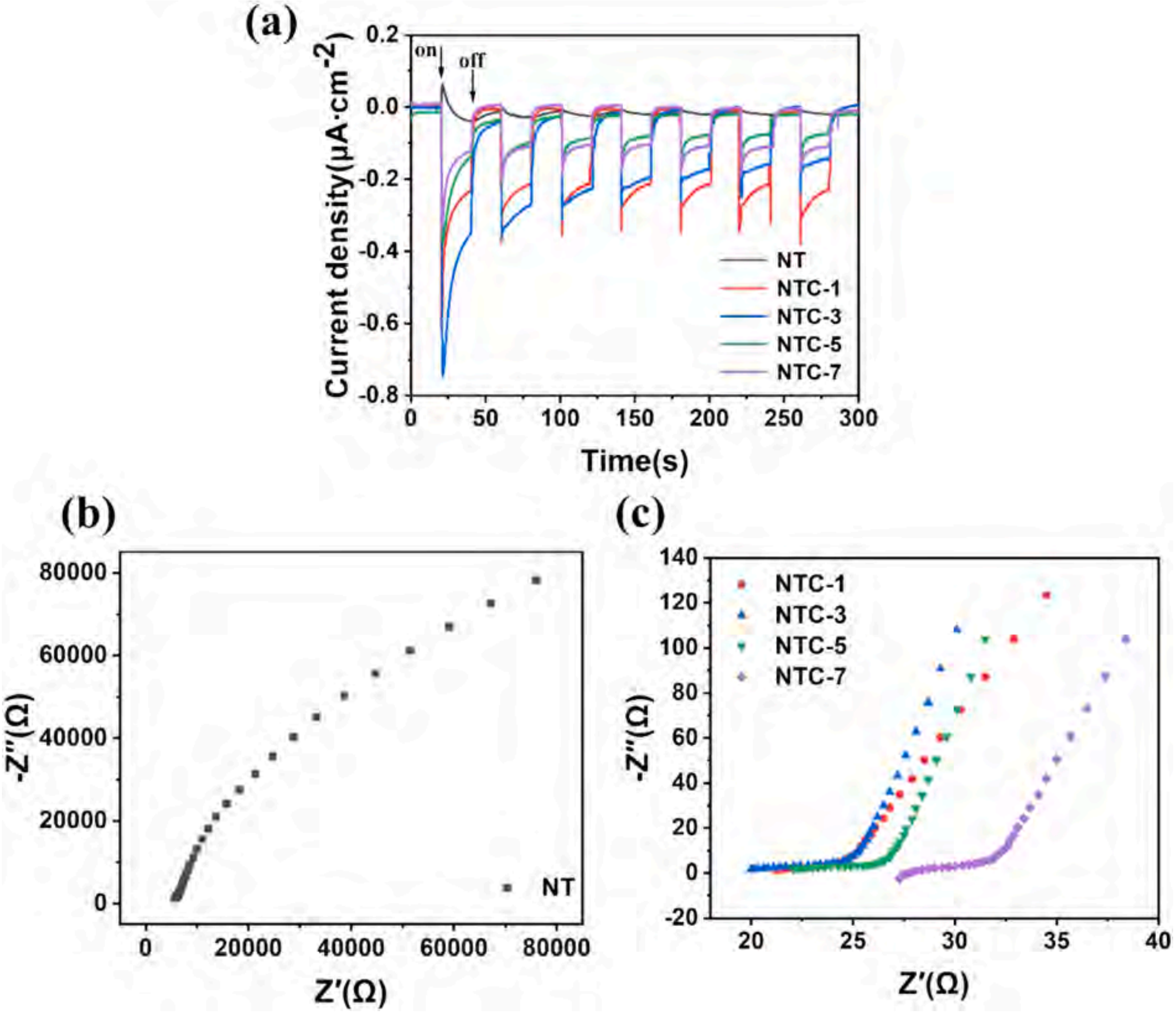

Fig. 6. (a) Transient photocurrent tests of NT and NTC-x under xenon lamp irradiation, (b) and (c) Electrochemical impedance spectroscopy of the samples.

Table 1
Transmittance of glass substrates coated with the samples.

Sample	380 ~ 760 nm Tave (%)		760 ~ 2500 nm Tave (%)		200 ~ 380 nm Tave (%)	
	blank glass	glass with coating	blank glass	glass with coating	blank glass	glass with coating
NT	95	95	83.1	83.1	90	90
NTC-1	95	95	83.3	83.2	90	91
NTC-3	95	95	83.4	82.9	90	89.8
NTC-5	95	95	83.3	82.4	90	89
NTC-7	95	95	83.3	82.7	90	89.9

coating effectively avoids the luminescence quenching of the upconversion luminescent nanoparticles caused by surface defects and residual ligands in the preparation process [35]. The introduction of CQDs doesn't significantly change the emission peak positions and enhances the intensity of the 545 nm, 548 nm and 657 nm emission peaks. The fluorescence decay lifetime at the strongest peak (666 nm) emitted by upconversion luminescence under 980 nm excitation is shown in Fig. 3b. The fluorescence decay lifetimes of NYF and NT at 666 nm are 191 μs and 532 μs. The coating of TiO_2 shell layer effectively suppressed the surface quenching and prolonged the fluorescence decay lifetime. Fig. 3c shows the CIE coordinates of the emission colors of (a) samples under 980 nm excitation. NYF emits mainly red light, while the shell coating enhances the energy transfer at higher energy levels of Er^{3+} and Tm^{3+} ions, changing the predominant emission color to green. Fig. 3d shows the down-conversion luminescence spectra of CQDs under 362 nm excitation and visible light emission (the peak located at 533 nm).

The schematic diagram of the mechanism of the upconversion luminescence system prepared in this work and energy transfer between rare earth ions and CQDs is shown in Fig. 4. The UCL route is as follows: the Yb^{3+} ions absorb the excited light at 980 nm to make electrons excite to higher level ($^2F_{7/2}\rightarrow{}^2F_{5/2}$) [36,37]. This energy is transmitted to the neighboring activator ions (Er^{3+} and Tm^{3+}) that absorb the energy to emit short-wavelength light through energy level transitions. The UCL peaks at 408 nm、520 nm、538 nm、651 nm、666 nm are respectively originated from the $^2H_{9/2}\rightarrow{}^4I_{15/2}$ [38]、 $^2H_{11/2}\rightarrow{}^4I_{15/2}$、$^4S_{3/2}\rightarrow{}^4I_{15/2}$ [39,40]、$^4I_{11/2}\rightarrow{}^4I_{15/2}$、$^4F_{9/2}\rightarrow{}^4I_{15/2}$ transitions of Er^{3+} ions [41,42]. The UCL peaks at 362 nm、451 nm、473 nm、699 nm are respectively originated from the $^1D_2\rightarrow{}^3H_6$ [43] 、 $^1D_2\rightarrow{}^3F_4$、$^1G_4\rightarrow{}^3H_6$、$^3F_3\rightarrow{}^3H_6$

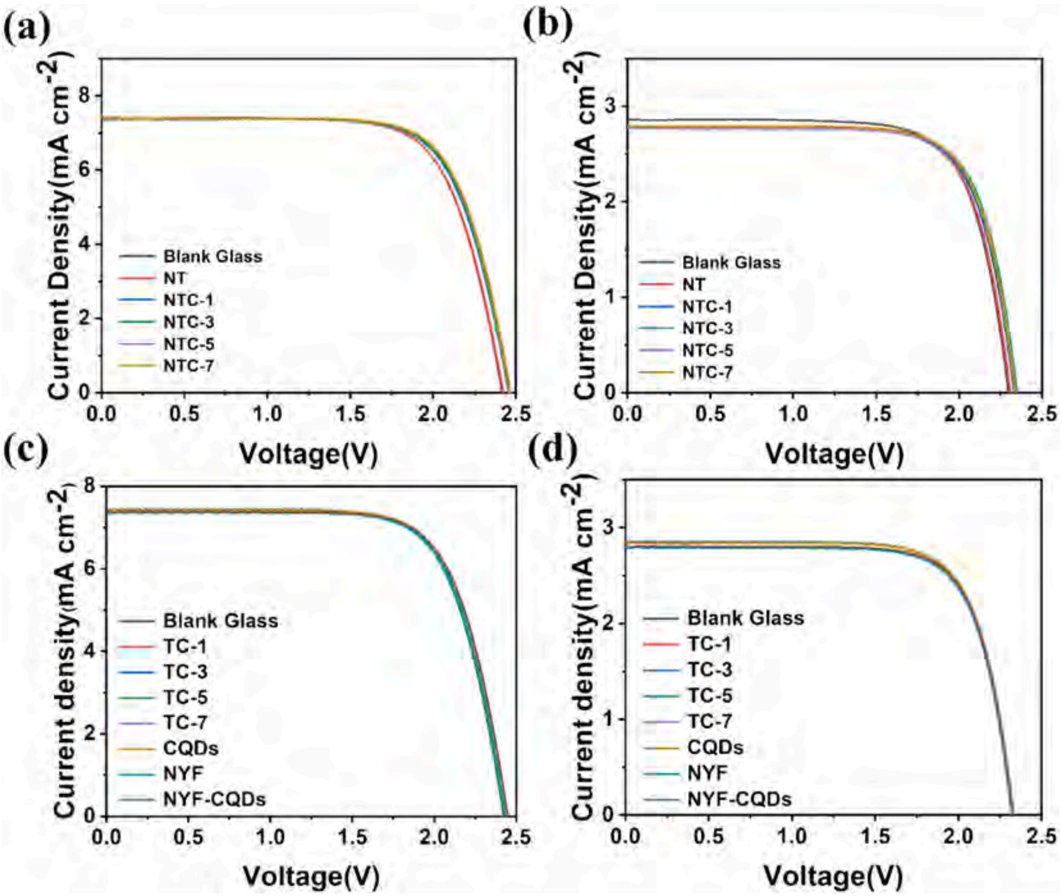

Fig. 7. J-V curves of as-prepared samples: (a) and (c) tested under sunlight, (b) and (d) tested under IR light.

Table 2
Electrical parameters of the solar cell covered with different samples under sunlight.

Sample	Jsc (mA cm^{-2})	Voc (V)	FF (%)	Eff (%)	overall increase (%)
Blank glass	7.41	2.42	72.10	12.91	
NT	7.40	2.42	72.08	12.92	0.08
NTC-1	7.37	2.46	72.66	13.14	1.78
NTC-3	7.38	2.46	72.91	13.22	2.40
NTC-5	7.38	2.47	72.04	13.30	3.02
NTC-7	7.39	2.46	73.03	13.31	3.10

Table 3
Electrical parameters of the solar cell covered with different samples under IR light (>760 nm).

Sample	Jsc (mA cm^{-2})	Voc (V)	FF (%)	Eff (%)	overall increase (%)
Blank glass	2.86	2.30	73.70	4.84	
NT	2.79	2.31	74.51	4.80	−0.83
NTC-1	2.77	2.33	74.76	4.83	−0.21
NTC-3	2.77	2.35	75.20	4.90	1.24
NTC-5	2.77	2.34	75.11	4.88	0.83
NTC-7	2.79	2.34	74.93	4.89	1.03

transitions of Tm^{3+} ions [44]. Through down-conversion luminescence, CQDs can absorb 362 nm UV light and convert it into 533 nm visible light. The 362 nm photons are exactly the ones emitted by up-converted nanoparticles that have a detrimental effect on photovoltaic cells, as prolonged UV exposure leads to the degradation of the performance of photovoltaic modules and the shortening of their lifespan.

As shown in Fig. 5a, b. The NT and NTC-x exhibit the intense light absorption in the ultraviolet section, which can be on account of charge transport process since valence to conduction in TiO_2 [45,46]. A blue shift in 350 nm for NTC-x is also clearly observed. Additionally, the peaks at 980 nm are absorption from Yb^{3+} [47]. The incorporation of CQDs with higher absorption into NT nanoparticles causes a remarkable absorption in the visible region [48].

According to Fig. 5a, the band gap energies (E_g) of the NT and NTC samples are calculate via the Kubelka-Munk equation [45]:

$$\beta h\nu = A(h\nu - E_g)^{1/2} \tag{1}$$

The E_g values of NT (2.95 eV), NTC-1 (2.99 eV), NTC-3 (2.99 eV), NTC-5 (2.84 eV) and NTC-7 (2.60 eV) are acquired from Fig. 5c.

The photoluminescence (PL) spectra of NT and NTC-x are presented in Fig. 5d. The excitation light source is 360 nm. The supernal PL emission signal of NT at 446.5 nm is owing to the quick recombination of electrons and holes of TiO_2. And the NTC-x show the junior PL release intensity, which means that photogenerated electrons and holes are separated and transferred more efficiently [49].

The transient photocurrent response of the samples is shown in Fig. 6a. Compared to NT, the photocurrent response values increase with the doped CQDs. The NTC-3 has the highest photocurrent response value at the beginning of illumination, and decreases with the extension of lighting time. The photocurrent response of NTC-1 is relatively high and stable. Besides, the NTC-x have lower electrochemical impedance values (Fig. 6b, c). The consequences indicate that NTC-x have the superior photogenerated electrons and holes separation and migration behavior. [50].

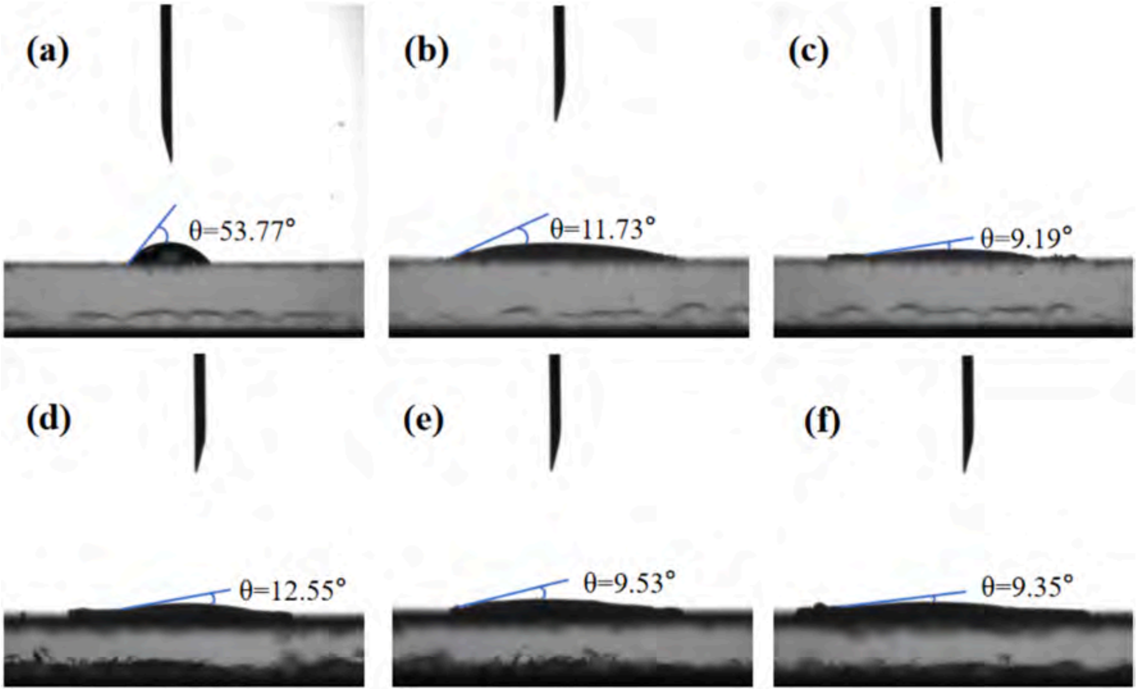

Fig. 8. Contact angle of water on (a) Glass without coating, (b) Glass with NT, (c) Glass with NTC-1, (d) Glass with NTC-3, (e) Glass with NTC-5, (f) Glass with NTC-7.

The transmittance of blank glass and glass coated with the as-prepared samples in three wavelength bands, UV light (200 ~ 380 nm), visible light (380 ~ 760 nm) and IR light (760 ~ 2500 nm), is shown in Table 1 and Table S1. The samples covered on glass exhibited no transmission loss in visible light, which assures that the PV cell efficiency will not be reduced after coating the samples.

Fig. 7 shows the J-V curves of the bare PV cell and the PV cell coated with the prepared coatings in a solar simulator by testing the variation of current density versus voltage of the PV cell. The PV cells did not show any significant change in performance from the graphs after coating the samples. The current density under infrared light irradiation is lower than that under sunlight irradiation, which is related to the photon absorption band of PV cells, because the main absorption peak of light in PV cells is visible light. And the detailed data differences will be described in Table 2 and Table 3. The meanings of the electrical parameters involved in the table are short circuit current density (Jsc), open circuit voltage (Voc), fill factor (FF) and efficiency (Eff) respectively. The overall increase Eff of PV cell with UCL nanoparticles (NT and NTC-1 to NTC-7) was compared to the bare PV cell covered glass sheet without UCL. Under 1 sun illumination, the photoelectric conversion efficiency (Eff) of PV cell is obviously improved with the increase of CQDs content. Compared to NT with an efficiency of 12.92 %, the overall efficiency of NTC-7 with an efficiency of 13.31 % is increased 3.02 % [51]. The efficiency in IR light is also significantly improved, indicating that the upconversion luminescence of the samples can convert IR light into visible light required by PV cell, and has a positive effect on the improvement of PV cell efficiency.

To demonstrate the synergistic effect of rare earth and CQDs, as a control, we tested samples with only CQDs (Table S2, S3). The results show that the efficiency of the samples with CQDs only (CQDs and TC-x) is lower than of the samples with rare earth and CQDs (NTC-x). The utilization wavelength of sunlight in photovoltaic cells is mainly concentrated in the visible light region, about 400 ~ 650 nm. Therefore, increasing the proportion of light in this band is obviously beneficial for improving the performance of photovoltaic cells. PV cells engaged photons of about 500 nm emitted by NYF for photoelectric conversion. According to the existing literature reports [52–54], CQDs can emit photons with a peak value of about 500 nm through the down conversion of 330 ~ 420 nm and upconversion of 590 ~ 1100 nm. At the same time, according to the data in Table 3 and Table S3, we believe that the ultraviolet light and red light emitted by $NaYF_4:Yb^{3+}/Er^{3+}/Tm^{3+}@TiO_2$ (NT) through the UCL process can be absorbed by CQDs and converted into photons to be absorbed and utilized by PV cells. *The comparison of the data related to the overall increase in efficiency of photovoltaic cell coated with different sample coatings can be seen directly in Fig. S5*. Thus, the luminescence synergy between $NaYF_4:Yb^{3+}/Er^{3+}/Tm^{3+}$ and CQDs allows PV cells to fully utilize those photons in the solar spectrum that cannot be absorbed, facilitating the efficiency enhancement of PV cells.

The contact angle of water droplets of the samples is shown in Fig. 8 [55]. Compared to glass without coating as shown in Fig. 8a, the contact angle of water droplets on glass with NT and NTC-x (Fig. 8b-f) decrease obviously [56], showing good hydrophilicity. It is easy for water spreads on the surface and picks up the soil [57], thus achieving the self-cleaning effect [58].

Further, the photocatalytic property was also perceived. The adsorption and photodegradation of acetaldehyde were measured in a continuous flow reactor system. The NT and NTC-x show excellent photocatalytic property under xenon lamp simulates sunlight irradiation that the degradation of acetaldehyde is more than 95 % in 1 h (Fig. S4a, b). Therefore, the prepared $NaYF_4:Yb^{3+}/Er^{3+}/Tm^{3+}@TiO_2$-CQDs upconversion luminescent nanoparticles not only could convert infrared light into visible light, but also have the hydrophilicity and the ability to remove volatile organic pollutants in the atmosphere. This not only has practical application prospects in the efficiency enhancement of photovoltaic cells, but also can be applied to the management of atmospheric pollutants to achieve multiple application effects.

4. Conclusion

In summary, we have successfully synthesized rare-earth doped TiO_2 core–shell structure and coupling CQDs to form the synergistic upconversion luminescence nanoparticles ($NaYF_4:Yb^{3+}/Er^{3+}/Tm^{3+}@TiO_2$-CQDs). The analysis reveals that the construction of core–shell structure greatly increases the UCL intensity through surface passivation, and mainly emits visible light (400 ~ 700 nm) under 980 nm excitation. The photogenerated electrons and holes of NTC-x are separated and transferred more efficiently comparing with NT. Under 1 sun illumination, the photoelectric conversion efficiency of PV cell with the as-prepared coatings is obviously improved (3.02 %). Besides, the material has good hydrophilic and photocatalytic degradation of acetaldehyde, which will be conducive to the realization of its self-cleaning performance and atmospheric pollutants removing. These results prove that the synergistic upconversion luminescence between rare earth and CQDs is beneficial for further improvement of PV cell efficiency and has a good application prospect in the green power domains.

CRediT authorship contribution statement

Shaoqi Zhu: Writing – original draft, Investigation, Data curation. **Xiaofeng Xie:** Writing – review & editing, Supervision, Funding acquisition, Conceptualization. **Xiaoyu Duan:** Resources, Methodology, Data curation. **Guanqing Song:** Validation, Software, Formal analysis. **Guanhong Lu:** Visualization, Resources, Methodology. **Yan Wang:** Validation, Methodology, Formal analysis. **Jing Sun:** Supervision, Resources, Project administration.

Declaration of competing interest

The authors declare that they have no known competing financial interests or personal relationships that could have appeared to influence the work reported in this paper.

Data availability

Data will be made available on request.

Acknowledgements

This work was supported by the National Natural Science Foundation of China (52072387); the Project of CHN Energy Investment Group (XNYGS-2023-422); Inner Mongolia Key R&D Plan (2022YFHH0049).

Appendix A. Supplementary data

Supplementary data to this article can be found online at https://doi.org/10.1016/j.jphotochem.2024.115866.

References

[1] Y. Gao, D. Wu, Z. Dai, C. Wang, B. Chen, X. Zhang, A comprehensive review of the current status, developments, and outlooks of heat pipe photovoltaic and photovoltaic/thermal systems, Renew. Energy 207 (2023) 539–574.

[2] P. Manisha, M. Kumari, R.K. Sahdev, S. Tiwari, A review on solar photovoltaic system efficiency improving technologies, Appl. Solar Energy 58 (2022) 54–75.

[3] A. Gholami, A.A. Alemrajabi, A. Saboonchi, Experimental study of self-cleaning property of titanium dioxide and nanospray coatings in solar applications, Sol. Energy 157 (2017) 559–565.

[4] A. Ghazy, M. Safdar, M. Lastusaari, H. Savin, M. Karppinen, Advances in upconversion enhanced solar cell performance, Sol. Energy Mater. Sol. Cells 230 (2021) 111234–111248.

[5] J. Zhang, L. Li, H. Li, Adsorption-controlled wettability and self-cleaning of TiO(2), Langmuir 39 (2023) 6188–6200.

[6] B.S. Richards, D. Hudry, D. Busko, A. Turshatov, I.A. Howard, Photon upconversion for photovoltaics and photocatalysis: a critical review, Chem Rev 121 (2021) 9165–9195.

[7] T. Zhang, L. Liu, R. Wang, W. Zhang, X. Liu, C. Yuan, R. Hua, Multi-color luminescence and anticounterfeiting application of upconversion nanoparticle, RSC Adv 13 (2023) 9273–9280.

[8] Y. Zhang, R. Wen, J. Hu, D. Guan, X. Qiu, Y. Zhang, D.S. Kohane, Q. Liu, Enhancement of single upconversion nanoparticle imaging by topologically segregated core-shell structure with inward energy migration, Nat Commun 13 (2022) 5927–5938.

[9] P. Du, P. Lei, Y. Liang, R. An, H. Zhang, New strategy: molten salt-assisted synthesis to enhance lanthanide upconversion luminescence, Small 19 (2023) 2302465–2302473.

[10] S. Liu, W. Li, S. Dong, F. Zhang, Y. Dong, B. Tian, F. He, S. Gai, P. Yang, An all-in-one theranostic nanoplatform based on upconversion dendritic mesoporous silica nanocomposites for synergistic chemodynamic/photodynamic/gas therapy, Nanoscale 12 (2020) 24146–24161.

[11] C. Sun, M. Gradzielski, Advances in fluorescence sensing enabled by lanthanide-doped upconversion nanophosphors, Adv Colloid Interface Sci 300 (2022) 102579–1025613.

[12] Q. Zhang, F. Yang, Z. Xu, M. Chaker, D. Ma, Are lanthanide-doped upconversion materials good candidates for photocatalysis? Nanoscale Horiz. 4 (2019) 579–591.

[13] F.T. Rabouw, P.T. Prins, P. Villanueva-Delgado, M. Castelijns, R.G. Geitenbeek, A. Meijerink, Quenching pathways in NaYF(4):Er(3+), Yb(3+) upconversion nanocrystals, ACS Nano 12 (2018) 4812–4823.

[14] J. Ma, Y. Wei, T. Liu, L. Xu, T. Wang, Z. Song, J. Qiu, Y. Li, Simultaneous enhancement upconversion luminescence and photocatalytic properties of BiOBr: Yb3+, Er3+ nanosheets by optically inert ions doping, J. Lumin. 260 (2023) 119860–119866.

[15] Y. Gao, S. Murai, K. Shinozaki, K. Tanaka, Up-conversion luminescence enhanced by the plasmonic lattice resonating at the transparent window of water, ACS Appl. Energy Mater. 4 (2021) 2999–3007.

[16] W. Gao, Z. Sun, Q. Han, S. Han, X. Cheng, Y. Wang, X. Yan, J. Dong, Enhancing upconversion emission of Er3+ in single β-NaYF4 microrod through constructing different inert and active shells with doping Yb3+ ions, J. Alloy. Compd. 857 (2021) 157578–157588.

[17] C. Mao, K. Min, K. Bae, S. Cho, T. Xu, H. Jeon, W. Park, Enhanced upconversion luminescence by two-dimensional photonic crystal structure, ACS Photonics 6 (2019) 1882–1888.

[18] P. Zhang, J. Ke, D. Tu, J. Li, Y. Pei, L. Wang, X. Shang, T. Guan, S. Lu, Z. Chen, X. Chen, Enhancing dye-triplet-sensitized upconversion emission through the heavy-atom effect in CsLu(2) F(7):Yb/Er nanoprobes, Angew. Chem. Int. Ed. Engl. 61 (2022) 202112125–202112132.

[19] G. Bao, S. Wen, W. Wang, J. Zhou, S. Zha, Y. Liu, K.L. Wong, D. Jin, Enhancing hybrid upconversion nanosystems via synergistic effects of moiety engineered NIR dyes, Nano Lett 21 (2021) 9862–9868.

[20] J. Wang, S. Zheng, H. Zhang, Y. Wu, Z. Jing, J. Liu, X. Zhu, Y. Zhang, Unraveling the growth process of core−shell structured upconversion nanoparticles: implications for color tuning of upconversion luminescence, Appl. Nano Mater. 6 (2023) 6398–6406.

[21] J. Huang, L. Yan, Z. An, H. Wei, C. Wang, Q. Zhang, B. Zhou, Cross relaxation enables spatiotemporal color-switchable upconversion in a single sandwich nanoparticle for information security, Adv Mater (2023) 2310524–2310532.

[22] L. Tian, Y. Shang, S. Hao, Q. Han, T. Chen, W. Lv, C. Yang, Constructing a "native" oxyfluoride layer on fluoride particles for enhanced upconversion luminescence, Adv. Funct. Mater. 28 (2018) 1803946–1803953.

[23] F. Zhao, X. Li, M. Zuo, Y. Liang, P. Qin, H. Wang, Z. Wu, L. Luo, C. Liu, L. Leng, Preparation of photocatalysts decorated by carbon quantum dots (CQDs) and their applications: a review, J. Environ. Chem. Eng. 11 (2023) 109487–109511.

[24] M.J. Molaei, Synthesis and application of carbon quantum dots derived from carbon black in bioimaging, J. Fluoresc. 34 (2023) 213–226.

[25] C. Yu, D. Li, W. Han, Y. Kong, L. Zhang, M. Chen, K. Hu, Improvement of photostability and thermal stability of PVC by carbon quantum dots loaded on TiO2, J. Vinyl Add. Tech. 29 (2023) 864–876.

[26] J. Gan, Y. Wu, F. Yang, H. Zhang, X. Wu, Y. Wang, R. Xu, Wood-cellulose photoluminescence material based on carbon quantum dot for light conversion, Carbohydr Polym 290 (2022) 119429–119437.

[27] G. Liu, M. Zavelani-Rossi, G. Han, H. Zhao, A. Vomiero, Red-emissive carbon quantum dots enable high efficiency luminescent solar concentrators, J. Mater. Chem. A 11 (2023) 8950–8960.

[28] X. Xu, W. Li, W. Zhou, G. Tan, Y. Zheng, C. Hu, B. Lei, X. Zhang, Y. Liu, J. Zhuang, Preparation and properties of dual-mode luminescent NaYF4:Yb, Tm@SiO2/carbon dot nanocomposites, J. Mater. Chem. C 6 (2018) 10360–10366.

[29] Z. Xu, M. Quintanilla, F. Vetrone, A.O. Govorov, M. Chaker, D. Ma, Harvesting lost photons: plasmon and upconversion enhanced broadband photocatalytic activity in core@shell microspheres based on lanthanide-doped NaYF4, TiO2, and Au, Adv. Funct. Mater. 25 (2015) 2950–2960.

[30] Y. Hu, X. Xie, X. Wang, Y. Wang, Y. Zeng, D.Y.H. Pui, J. Sun, Visible-light upconversion carbon quantum dots decorated TiO2 for the photodegradation of flowing gaseous acetaldehyde, Appl. Surf. Sci. 440 (2018) 266–274.

[31] M. Meng, R. Zhang, X. Fa, J. Yang, Z. Cheng, A.A. Ansari, J. Ou, C. Wurth, U. Resch-Genger, Preparation of core-shell structured NaYF4:Yb3+/Tm3+@NaYF4:Yb3+/Er3+ nanoparticles with high sensitivity, low resolution and good reliability and application of their fluorescence temperature properties, CrstEngComm 24 (2022) 1752–1763.

[32] J. Xia, F. Wang, M. Zhou, K. Lu, W. Huang, C. Yu, K. Yang, Facile synthesis of VS2/CdS/NaYF4: Yb, Er ternary heterojunctions for the visible-near-infrared-light driven photocatalysis, J. Solid State Chem. 317 (2023) 123583–123593.

[33] G. Lu, X. Wang, Y. Wang, G. Shi, X. Xie, J. Sun, Anti-oxidative microstructure design of ultra-stable N-TiO2 composite for the gaseous photodegradation reactions, Chem. Eng. J. 408 (2021) 127257–127266.

[34] P. Chen, F. Wang, Z.-F. Chen, Q. Zhang, Y. Su, L. Shen, K. Yao, Y. Liu, Z. Cai, W. Lv, G. Liu, Study on the photocatalytic mechanism and detoxicity of gemfibrozil by a sunlight-driven TiO2/carbon dots photocatalyst: the significant roles of reactive oxygen species, Appl Catal B 204 (2017) 250–259.

[35] W. Gao, Y. Xing, B. Chen, L. Shao, J. Zhang, X. Yan, Q. Han, C. Zhang, L. Liu, J. Dong, Enhancing red upconversion emission in NaErF4@NaYF4 core-shell nanoparticles by introducing Yb3+ ions as energy trapping centers, J. Alloy. Compd. 936 (2023) 168371–168380.

[36] S. Zeng, G. Ren, W. Li, C. Xu, Q. Yang, Highly uniform Tm3+-doped NaYbF4 microtubes: controlled synthesis and intense ultraviolet photoluminescence, J. Phys. Chem. C 114 (2010) 10750–10754.

[37] S. Zeng, G. Ren, W. Li, C. Xu, Q. Yang, Highly uniform Tm3+ doped NaYbF4 microtubes: controlled synthesis and intense ultraviolet photoluminescence, J. Phys. Chem. C 114 (2010) 10750–10754.

[38] T. Sun, Y. Li, W.L. Ho, Q. Zhu, X. Chen, L. Jin, H. Zhu, B. Huang, J. Lin, B.E. Little, S.T. Chu, F. Wang, Integrating temporal and spatial control of electronic transitions for bright multiphoton upconversion, Nat. Commun. 10 (2019) 1811–1817.

[39] Y. Wang, W. Lu, D. Yue, M. Wang, B. Tian, Q. Li, B. Hu, Z. Wang, Y. Zhang, A strategy to enhance the up-conversion luminescence of nanospherical, rod-like and tube-like NaYF4: Yb3+, Er3+ (Tm3+) by combining with carbon dots, CrstEngComm 23 (2021) 935–943.

[40] S. Namagal, N. Victor Jaya, N. Nithyaa, M. Muralidharan, S. Venkatesh, Upconversion of NaYF4: Yb, Er nanoparticles Co-doped with Zr 4+ for magnetic phase transition and biomedical imaging applications, J. Inorg. Organomet. Polym Mater. 32 (2022) 3128–3140.

[41] S.-Y. Sun, Y.-Y. Ge, Y.-J. Zhao, Z.-P. Xie, Synthesis of Er3+ doped KNbO3 nanocrystals and nanoceramics with outstanding up-conversion luminescence behaviors, J. Alloy. Compd. 854 (2021) 156738–156744.

[42] J. Sun, F. Lai, J. Chen, L. Ke, X. Shi, C. Li, B. Wang, Y. Qiang, W. You, Effect of local crystal field environment on luminous properties of Er3+/Yb3+-doped titanate upconversion luminescent materials, J. Lumin. 255 (2023) 119590–119596.

[43] Y. Tang, W. Di, X. Zhai, R. Yang, W. Qin, NIR-responsive photocatalytic activity and mechanism of NaYF4:Yb, Tm@TiO2 core-shell nanoparticles, ACS Catal. 3 (2013) 405–412.

[44] Y. Zhang, X. Lan, S.H. Park, L. Wang, D. Liu, J. Shi, Rational design of efficient near-infrared photon conversion channel via dual-upconversion process for superior photocatalyst, Carbon 169 (2020) 111–117.

[45] C. Jia, X. Kan, X. Zhang, G. Lin, W. Liu, Z. Wang, S. Zhu, D. Ju, J. Liu, Construction of frustrated Lewis pairs on TiO2-x derived from perovskite for enhanced photocatalytic CO(2)reduction, Chem. Eng. J. 427 (2022) 131554–131562.

[46] P. Mazierski, A. Mikolajczyk, T. Grzyb, P.N.A. Caicedo, Z. Wei, E. Kowalska, H. P. Pinto, A. Zaleska-Medynska, J. Nadolna, On the excitation mechanism of visible responsible Er-TiO2 system proved by experimental and theoretical investigations for boosting photocatalytic activity, Appl. Surf. Sci. 527 (2020) 146815–146825.

[47] Z. Nie, X. Ke, D. Li, Y. Zhao, L. Zhu, R. Qiao, X.L. Zhang, NaYF4:Yb, Er, Nd@NaYF4: Nd upconversion nanocrystals capped with Mn:TiO2 for 808 nm NIR-triggered photocatalytic applications, J. Phys. Chem. C 123 (2019) 22959–22970.

[48] A. Mozdbar, A. Nouralishahi, S. Fatemi, F.S. Talatori, The impact of carbon quantum dots (CQDs) on the photocatalytic activity of TiO2 under UV and visible light, J. Water Process Eng. 51 (2023) 103465–103476.

[49] Y. Huang, Z. Yu, P. Wang, S. Li, Q. Tan, N. He, Q. Xiang, Sulfur-modulated metal–organic framework MIL-101(Fe) with CQDs anchored as an efficient light-driven photocatalyst: photocatalytic performance and mechanism investigation, New J. Chem. 47 (2023) 6804–6821.

[50] J. Fang, H. Wei, Y. Chen, B. Dai, Y. Ni, J. Kou, C. Lu, Z. Xu, Low-energy photons dual harvest for photocatalytic hydrogen evolution: bimodal surface plasma resonance related synergism of upconversion and pyroelectricity, Small 19 (2023) 2207467–2207476.

[51] Y.N. Chouryal, R.K. Sharma, N. Tomar, N. Yadav, H.L. Kewat, I.A. Wani, S. Nigam, P.K. Surolia, S. Sivakumar, P. Ghosh, Upconverted nanophosphors for increasing efficiency in a dye-sensitized solar cell, ACS Applied Energy Materials 6 (2023) 4934–4941.

[52] F. Duo, Y. Wang, C. Fan, X. Zhang, Y. Wang, Enhanced visible light photocatalytic activity and stability of CQDs/BiOBr composites: the upconversion effect of CQDs, J. Alloy. Compd. 685 (2016) 34–41.

[53] X. Xu, Z. Bao, G. Zhou, H. Zeng, J. Hu, Enriching photoelectrons via three transition channels in amino-conjugated carbon quantum dots to boost photocatalytic hydrogen generation, ACS Appl. Mater. Interfaces 8 (2016) 14118–14124.

[54] W. Gao, S. Zhang, G. Wang, J. Cui, Y. Lu, X. Rong, C. Gao, A review on mechanism, applications and influencing factors of carbon quantum dots based photocatalysis, Ceram. Int. 48 (2022) 35986–35999.

[55] S.I. Hussein, M.M. Hassin, Study the Effect of graphene on the contact angle, water absorption and thermal stability (TGA, DSC) for blend (Epoxy & Repcoat ZR), Iraqi J. Phys. (IJP) 19 (2021) 43–50.

[56] T. Zhang, J. Sun, H. Zhou, Z. Wang, D. Yang, F. Qiu, Biomass cellulose aerogel composites with functional integration for thermal insulation applications, J. Sol-Gel Sci. Technol. 109 (2023) 110–118.

[57] A.S. Sarkın, N. Ekren, Ş. Sağlam, A review of anti-reflection and self-cleaning coatings on photovoltaic panels, Sol. Energy 199 (2020) 63–73.

[58] H. Lu, B. He, W. Zhao, Experimental study on the super-hydrophobic coating performance for solar photovoltaic modules at different wind directions, Sol. Energy 249 (2023) 725–733.